Stress release waves in plastic solids

Gilles Damamme, Joris Vermunt, Don-Pierre Zappa, Helmut Klöcker

Stress Release Waves in Plastic Solids

Gilles Damamme[1], Joris Vermunt[1], Don-Pierre Zappa[1], Helmut Klöcker[2]

[1]CEA, DAM, CEA-GRAMAT, F-46500 Gramat, France

[2]ENSMSE, F-42023 Saint-Etienne, France

ABSTRACT

Better understanding of damage under high strain rate deformation is critical; whether assessing the impact of new weapon systems, calculating safety issues, or even modelling modern high speed machining. Mott waves, one of the keystones needed to predict bomb debris size, are reexamined. Mott assumed instantaneous through thickness crack propagation and stress relaxation waves unloading the material surrounding the crack. But, following experimental evidence, crack extension velocity actually has limits. A new energy balance based framework, considering damage development during stress release waves propagation is presented. Exact boundaries for the time and wave position at failure are established. Particular wave paths close to these boundaries are analyzed. This work will be the basis to predict more accurately fragment size distributions having industrial as well as military applications.

KEYWORDS

Mott's wave, Boundaries, Energy approach, Fragmentation, Failure energy, Dynamic, Ductile material

Corresponding author
Prof. Helmut Klöcker
Ecole des Mines
158 Cours Fauriel
42023 Saint Etienne
France
klocker@emse.fr

1. Introduction

At the onset of World War II, fragmentation studies of expanding cylinders, were being used to predict the debris distribution for conventional warheads. In 1943, Mott and Linfoot extended Lienau's

1

purely mathematical line break-up model (Lienau, 1936) to develop the initial theory of dynamic plate fragmentation (Mott and Linfoot, 1943). Soon after, Mott made a conceptual breakthrough by deciding to consider the cylinder as a stack of steel rings. With this brilliant hypothesis and the introduction of several probability distributions of initial defects, he was able to successfully predict fragment mass scattering (Mott 1943, 1944, 1947). Right from the beginning, Mott considered stress relaxation waves, which are now named in his honor. Mott waves are one of the foundations needed to predict bomb debris size because once unloaded, the parts of shell casings no longer fracture.

Unfortunately, given the computational limits of the 1940s, Mott was required to simplify crack propagation through thickness as instantaneous. That implied that the load carrying capacity of the corresponding section drops to zero, which Mott knew was an oversimplification.

In quasi-static deformation (small strain rates), ductility increases fracture energy and as consequence slows down crack propagation (Freund (1985), Tvergaard and Needleman (1984), Zhang and Ravi-Chandar (2006, 2008), Gao (2005), Levy (2010)). Thus, the first step was to experimentally demonstrate the existence of ductile failure even at very high strain rates. Based on his theoretical and experimental work on expanding tubes, Taylor demonstrated that, before breaking, the mean strain is around 60% (Taylor, 1963). Ductile failure requires lots of energy (Nemat-Nasser et al. (1983)) and consequently leads to slow crack propagation. Ergo, yielding and strain hardening influence fragmentation and Mott's model had to be enhanced. To the best of our knowledge, Grady who has published numerous papers and books in this field, was the very first to deal with non-instantaneous crack propagation (Grady, 1982). Hence, he was able to predict the mean mass of the fragments but not their mass distribution (Grady 1982, 2006).

Zhou et al. (2005) analyzed the fragmentation process in a one-dimensional bar taking into account elastic wave interaction and considering a cohesive crack opening process. They applied the model to a prototypical ceramic bar. For very high strain rates, Zou et al predict an average fragment size about 5 times smaller than the Grady. Levy et al. (2010) simulated the fragmentation of a uniformly expanding ring within a finite element framework, coupled to linear cohesive elements. They suggest the distribution of fragment masses follows a universal curve, which depends only on the average fragment mass. . Cereceda et al. (2017) used the model suggested by Zhou et al. to assess dynamic fragmentation in glass, concrete and masonry.

Unfortunately, all attempts to consider damage were based on ad hoc additions of an internal stress to Mott's original model or finite element analyses. Present work offers a new model by coupling Mott's wave and progressive damage based on minimalist assumptions. Only positive energy dissipation during failure will be assumed.

2. Mott's model and Grady's extension

Mott investigated the dynamics of an infinite plastic rod. Prior to crack nucleation, the rod undergoes a homogeneous, time dependent, uniaxial strain rate, $\dot{\varepsilon}_{11}(x,t) = \dot{\varepsilon}_{11}(t) = \partial v/\partial x$. The uniaxial velocity $v(x,t)$ depends linearly on the x coordinate. The velocity v, constant over time at any material location X, is a convenient Lagrangian variable given by:

$$v(x,t) = \dot{\varepsilon}_{11}(t)x = \dot{\varepsilon}X \tag{1}$$

$\dot{\varepsilon}$ is the initial straining rate.

Mott considered crack nucleation, at $t = \tau$, leading to instantaneous through thickness propagation separating the rod in two: a stress partially released and a loaded part (Fig. 1a). The moving interface between these two parts is called a Mott wave. These waves prevent further damage nucleation because of the stress partially released volume they produce. The material beyond section B undergoes uniform expansion. The material between the crack (0) and the moving interface B is partially unloaded. Mott modelled the material as perfectly plastic after through thickness crack propagation:

$$Y(t \geq \tau) = Y(\tau) = \sigma_Y \tag{2}$$

Beyond B the material is submitted to σ_Y. The stress increases linearly between sections A and B. Newton's second law of motion and mass conservation imply the following equation for the velocity

$$v\,t\left(\frac{dv}{dt}\right) = \frac{\sigma_Y}{\rho} \tag{3}$$

The wave front position X_M is given by

$$X_M = \sqrt{D\,\tau}\quad D = \frac{2\,\sigma_Y}{\rho\,\dot{\varepsilon}} \tag{4}$$

With this simple model, combined with adequate assumptions concerning damage nucleation, Mott estimated the fragment distribution of steel warheads by hand. The lack of computers forced Mott to oversimplify the physical problem. The most significant limitation is the assumption of instantaneous through thickness crack propagation.
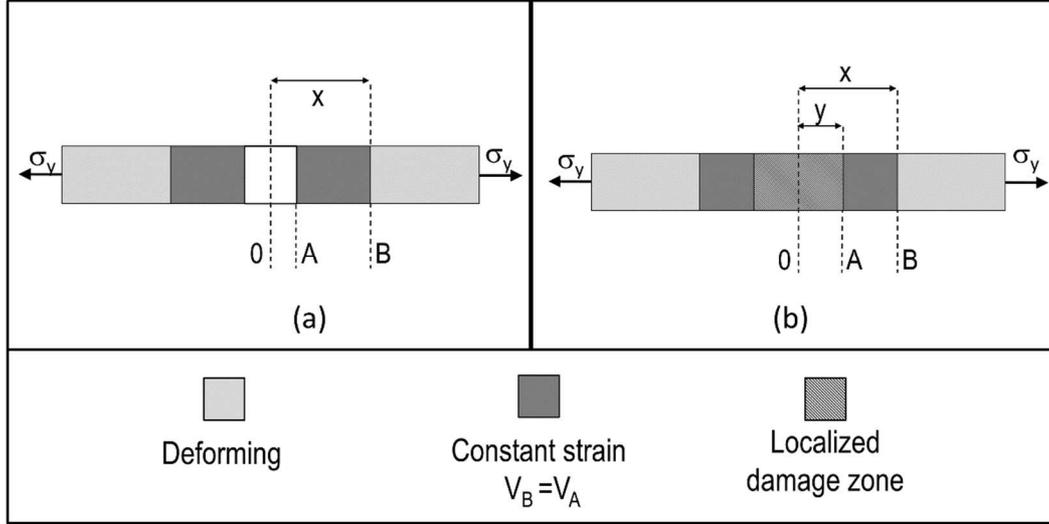
Fig.1 *(a) Original Mott's model (b) Grady's extension of Mott's model*

Grady has offered an extension of Mott's model, including delayed crack opening, based on the remaining load carrying capacity σ_Y φ (Fig. 1b). As before, unloading waves are still considered as propagating from section A to section B. At section B, the rod is submitted to the stress σ_Y and in section A, the stress is reduced to σ_Y φ. Between sections A and B, postulating the strain remains constant. Newton's second law, mass conservation and equation (4) give the wave front velocity:

$$\frac{d(v^2)}{d\varepsilon} = \frac{\sigma_Y}{\rho} \varphi(y) \tag{5}$$

Identical velocities at sections A and B, give a simple relation between the wave front velocity v and the new internal damage variable y:

$$v = \frac{dy}{dt} \tag{6}$$

All the mass is assumed to be between y and x. The remaining load carrying capacity of all the volume delimited by the initial defect (crack in section A) and the wave front (B) is thus described by a single variable y and the associated function φ. For a linear damage function, Grady predicts the time and wave position at failure as:

$$t_r = \left(\frac{72\rho\Gamma^2}{\sigma_y^3}\right)^{\left(\frac{1}{3}\right)} \quad X_r = \left(\frac{3\Gamma}{\rho\dot{\varepsilon}^2}\right)^{\left(\frac{1}{3}\right)} \tag{7}$$

Where Γ is the fragmentation energy

Grady made major contributions to dynamic failure. His work leads to deeper insight of the synergy between damage growth (through thickness crack development) and stress release wave propagation. Unfortunately, equations (5) and (6) lead to simple solutions only for a very limited choice of damage potentials. Moreover, the ad hoc introduction of a non-zero interface stress should be justified. In contrast, our comprehensive energy based approach, presented in the next section assumes positivity energy dissipation during through-thickness failure development.

4

3. Energy balance based extension of Mott's Model

3.1. Energy balance

Similarly, to Mott and Grady, we consider a rod, submitted to homogeneous strain rate $\dot{\varepsilon}$, experiencing damage nucleation at $t = t_i$ ($\tau = 0$). In the material ahead of the stress relaxation front, the dissipated power per unit volume is given by $\sigma_y \dot{\varepsilon}$. If X stands for the wave front position at time τ, an energy balance applied to the material $[0, X(\tau)]$ between the times 0 and τ leads to:

$$\rho \dot{\varepsilon}^2 \frac{X^3}{6} + \sigma_y \dot{\varepsilon} X \tau = \frac{1}{2} \rho \dot{\varepsilon}^2 X^3 + \gamma(\tau) + \sigma_y \dot{\varepsilon} \int_0^\tau t \, dX \tag{8}$$

The two terms on the left side of the equation, correspond respectively to the initial kinetic energy and the external work rate. The terms on the right side relate respectively to the final kinetic energy, the energy dissipated to damage the material and the energy dissipated by plastic deformation. Integration by parts leads to the following expression for the wave front position X

$$\sigma_y \dot{\varepsilon} \int_0^\tau X(t) \, dt = \gamma(\tau) + \frac{1}{3} \rho \dot{\varepsilon}^2 X^3(\tau) \tag{9}$$

Recently, Vocialta et al. (2015) considered possible friction between debris by a cohesive zone based f.e. analysis. In present approach, friction affect the energy dissipated to damage the material.

3.2. Wave front delay compared to Mott's solution

Deriving equation (9) with respect to the time and rearranging the different terms leads to

$$\rho \dot{\varepsilon}^2 X^2(\tau) \dot{X} = \sigma_y \dot{\varepsilon} X(\tau) - \dot{\gamma}(\tau) \tag{10}$$

$\dot{\gamma}$ designates the power dissipated in the damaging process. Consistent with the assumption of a perfectly plastic material, we assume the dissipated energy depends only on the wave front position. Hence, previous equation leads to a simple relation between the wave front position and the dissipation:

$$\frac{d\gamma}{dX} = \sigma_y \dot{\varepsilon} \left(X \frac{d\tau}{dX} - \frac{2 X^2}{D_{Mott}} \right) \quad \text{where} \quad D_{Mott} = \frac{2\sigma_y}{\rho \dot{\varepsilon}} \tag{11}$$

After complete failure($\tau \geq \tau_r$), the energy dissipated in the damaging process remains constant ($\dot{\gamma} = 0$). So, equation (10) simplifies to Mott's equation.

$$\frac{d(X^2)}{d\tau} = D_{Mott} \tag{12}$$

The solution to equation (12) corresponds to a delayed Mott wave:

$$X^2 = D_{Mott}(\tau - \tau_d^r) \tag{13}$$

Where τ_d^r represents the wave front compared to Mott's solution (with zero energy dissipation) at failure.
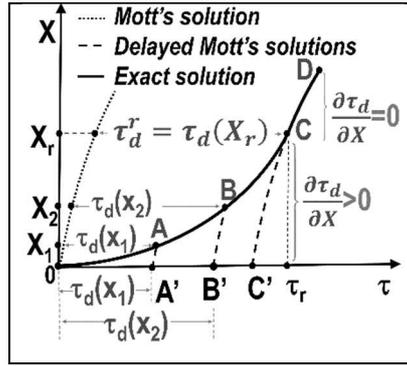
Figure 2: Real wave front position (X, τ)

Figure 2 is a schematic representation of the real wave front positon. Every point in the (X, τ) −space may be reached by a delayed Mott wave:

$$X^2 = D_{Mott}[\tau - \tau_d(X)] \quad or \quad \tau_d(X) = \tau - \frac{X^2}{D_{Mott}} \tag{14}$$

Combining the last expression with equation (11) puts forward a simple relation between the increase in dissipated energy and time delay

$$\frac{d\gamma}{dX} = \sigma_y \, \dot{\varepsilon} \, X \left(\frac{d\tau_d}{dX}\right) \tag{15}$$

Therefore, the delay $\tau_d(X)$ depends on the current wave front position X. Hence, the wave front position (10) may be expressed as a function of the energy dissipation rate, the yield strength and the remote strain rate:

$$\frac{d(X^2)}{d\tau} = D_{Mott}\left[1 - \frac{\dot{\gamma}(\tau)}{\sigma_y \, \dot{\varepsilon} X(\tau)}\right] \tag{16}$$

Combining the two previous equations provides a relation between the derivative of τ_d and the power dissipated to damage the material $(\dot{\gamma})$

$$\frac{d\tau_d}{d\tau} = \frac{\dot{\gamma}(\tau)}{\sigma_y \, \dot{\varepsilon} X(\tau)} \tag{17}$$

$\sigma_y \, \dot{\varepsilon} X(\tau) d\tau_d$ is the energy used to damage the material during the time $d\tau$. As X > 0 and $\dot{\gamma} \geq 0$, the derivative of the time delay is always positive, and τ_d increases from 0 to its maximum τ_d^r.

3.3. Stress and damage variable

The interface (y) between the localized damage zone and the rigid material governs damage evolution. Its velocity, $\dot{y}$, describes damage progression, whereas y corresponds to its accumulation. Assuming rigid plastic behavior leads to:

$$\dot{y} = \dot{\varepsilon} \, X, \quad y = \int_0^\tau \dot{\varepsilon} \, X(t)dt \tag{18}$$

The stress σ associated to y than naturally follows from the dissipated power:

$$\dot{\gamma}(\tau) = \sigma(\tau)\dot{y} = \sigma(\tau)\dot{\varepsilon} \, X(\tau) \tag{19}$$

6

Hence, σ is related to the variation of the time delay:

$$\sigma(\tau) = \frac{1}{\dot{\varepsilon}\,X(\tau)}\frac{d\gamma}{d\tau} = \sigma_Y\frac{d\tau_d}{d\tau} \tag{20}$$

The stress depends on the remote strain rate, the wave front position and the energy dissipation rate. Equations (9) and (18) lead to a simple expression of the damage variable y.

$$y = \int_0^\tau X(t)\,dt = \frac{\gamma(\tau)}{\dot{\varepsilon}\,\sigma_Y} + \frac{1}{3}\frac{\rho\,\dot{\varepsilon}\,X^3(\tau)}{\sigma_Y}$$

$$y(\tau) = \frac{\gamma(\tau)}{\dot{\varepsilon}\,\sigma_Y} + \frac{2\dot{\varepsilon}}{3D_{Mott}}\,X(\tau)^3 \quad D_{Mott} = \frac{2\sigma_y}{\rho\dot{\varepsilon}} \tag{21}$$

The variable, y, depends on the energy dissipated to damage the material, the wave front position and the strain rate. The new model includes Mott's original approach ($\dot{\gamma} = 0$), but shows clearly the need to incorporate a second characteristic value ($\dot{\gamma}/\,\sigma_y\,\dot{\varepsilon}X$). This quantity measures the ratio between energy dissipation rate and total power. Equations (20) and (21) define damage evolution. The parameter τ may eventually be eliminated for particular (X,τ) −curves. Before doing so, the limitations to all possible (X,τ) −curves are analyzed.

3.4. Allowable damage laws and characteristic lengths

Consistent with the assumption of rigid plastic material, we hypothesize that dissipated power depends solely on the damage variable y.

$$\left.\frac{\partial\gamma}{\partial\dot{\varepsilon}}\right]_y = 0 \tag{22}$$

To analyze the impact of this hypothesis, we introduce the reduced time T and wave front position χ by:

$$T = \tau\,\dot{\varepsilon}^{(-n)} \quad X = \dot{\varepsilon}^m\,\chi \tag{22}$$

Equation (10) transforms into:

$$\rho\,\dot{\varepsilon}^{(2+3m-n)}\,\chi^2(T)\chi'(T) = \sigma_y\,(\dot{\varepsilon})^{(1+m)}\,\chi(T) - (\dot{\varepsilon})^{(-n)}\gamma'(T)$$

χ' represents the derivative of χ with respect to T. Hence, invariance of equation (10) with respect to $\dot{\varepsilon}$ implies:

$$\begin{cases} 2 - n + 3m = 1 + m \\ 2 - n + 3m = -n \end{cases}$$

The second expression, $(2 - n + 3m = -n)$, is due to energy dissipation and thus not present in Mott's original approach.. The new model (with $m = -2/3$ and $n = -1/3$) leads to:

$$T = \tau\,\dot{\varepsilon}^{(1/3)} \quad X = \dot{\varepsilon}^{\left(-\frac{2}{3}\right)}\chi \tag{23}$$

In the (χ, T)-space, the relation between wave front position and time does no more depend on the strain rate:

$$\begin{cases} \dfrac{d(\chi^2)}{dT} = D\left[\, 1 - \dfrac{\gamma'}{\sigma_Y \chi}\right] \\ D = D_{MOTT}\dot{\varepsilon} = \dfrac{2\sigma_Y}{\rho} \end{cases} \quad \text{where } \gamma' = \dfrac{d\gamma}{dT} \tag{24}$$

In the (χ, T) −space, the physical parameter, D (m²/s²), corresponding to Mott's initial solution is independent of the strain rate. The new time delay, coherent with equation (23), leads to a simpler expression of the stress

$$T_d(T) = \dot{\varepsilon}^{\,1/3}\tau_d(\tau) \ \ and \ \ \sigma(T) = \frac{1}{\chi}\left(\frac{d\gamma}{dT}\right) = \sigma_y\left(\frac{dT_d}{dT}\right) \tag{25}$$

As a consequence of equation (24) any possible (χ, T)-curve corresponds to a delayed Mott path. Furthermore, continuity of the dissipated energy γ implies continuity of the wave front position $\chi(T)$. Figure 3 illustrates this condition. If all material parameters $(\Gamma, \sigma_Y, X_r, \tau_r)$, as well as the loading $(\dot{\varepsilon})$ are fixed, an infinity of solutions is still possible. Among these, Grady has chosen power laws.
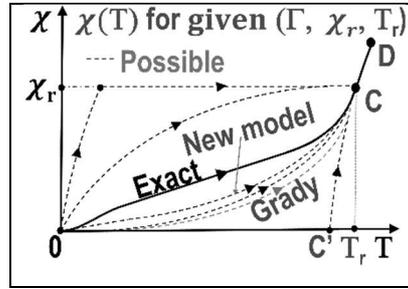

Figure 3: Acceptable $(\boldsymbol{X}, \boldsymbol{\tau})$-curves

Equation (24) leads to an explicit relation between the time and wave front position:

$$\frac{dT}{d\chi} = \frac{2\chi}{D}\left[\, 1 - \frac{\gamma'}{\sigma_Y\, \chi}\right]^{-1} \ \rightarrow \ \frac{dT}{d\chi} \geq \frac{2\chi}{D} \tag{26}$$

If the reduced dissipated power ($\gamma'/\sigma_Y\, \chi$) is a function of the wave front position, the latest satisfies:

$$T = \frac{2}{D}\int_0^{\chi} \frac{dx}{\left[\, 1 - \frac{\gamma'}{\sigma_Y\, x}\right]} \tag{27}$$

Without explicit knowledge of $\gamma'(x)$ in function of, previous equation may not be integrated. However, the allowed (χ, T)- domain may be bounded. Irreversibility implies $\gamma' \geq 0$. Hence, Mott's un-delayed solution ($\gamma' = 0$) corresponds to a lower limit of the $\chi(T)$ curves (B$_1$ in figure 4). Moreover, for a given time delay at failure (T_d^r), inequality (26) gives an upper bound to $\chi(T)$. Figure 4 shows the allowable domain in the (χ, T)-space. Both boundaries may be expressed as delayed Mott's waves:

$$\begin{cases} B_1 \equiv T = \dfrac{\chi^2}{D} + T_d^r H(\chi - \chi_r) \\ B_2 \equiv T = \dfrac{\chi^2}{D} + T_d^r H(\chi) \end{cases} \tag{28}$$

Figure 4: Allowed domain in the (X, τ)-space

Bounding the possible (χ, T)-curves, naturally leads to a new relation between the total dissipated energy at failure Γ and the (χ_r, T_r) coordinates. By relation (15), the total energy dissipated to damage the material is:

$$\Gamma = \gamma(T_r) = \sigma_Y \int_0^{\chi_r} \chi \frac{dT_d}{d\chi} \, d\chi \tag{29}$$

Equation (29) leads to a geometrical interpretation of the failure energy (Figure 5). Γ/σ_Y corresponds to the area bounded to the left by the exact solution (OC) and to the right by the delayed Mott's wave passing through the same point C (C'C).

Figure 5: Geometrical interpretation of the failure energy r

For both boundaries, the previous yields:

$$\begin{cases} B_1^r : \Gamma = (\sigma_Y) T_d^r \int_0^{\chi_r} \chi \, \delta(\chi - \chi_r) \, d\chi = 0 \\ B_2^r : \Gamma = (\sigma_Y) T_d^r \int_0^{\chi_r} \chi \, \delta(\chi) \, d\chi = (\sigma_Y) T_d^r \chi_r \end{cases} \tag{30}$$

Hence, the total energy dissipated to failure the material, Γ has to satisfy the following inequality:

$$0 < \Gamma < \sigma_Y \left(\chi_r T_r - \frac{\chi_r^3}{D} \right) \tag{31}$$

For a specified value of the failure energy Γ, previous equation involves a lower bound to the time to failure as a function of the corresponding wave front position.

$$T_r > \frac{\chi_r^2}{D} + \frac{D_2}{3\chi_r} = \frac{\chi_r^2}{D} + T_d^r \quad \text{with } D_2 = \frac{3\Gamma}{\sigma_Y} \tag{32}$$

The first term on the right corresponds to a non-delayed Mott wave, whereas the second measures the time needed to transfer enough energy to failure the material. D_2 has the dimension of a length. Taking into account the failure energy leads naturally to the introduction of a characteristic length scale D_2.

A new lower bound to the fracture time can be established by requiring a positive value for the interface stress and negative value for its derivative with respect to the damage variable.

$$\begin{cases} \sigma(y) \geq 0 \\ \frac{d\sigma(y)}{dy} \leq 0 \end{cases} \tag{33}$$

Remembering equation (25), the previous conditions lead to

$$\begin{cases} \frac{dT_d}{dT} \geq 0 \\ \frac{d^2 T_d}{dT^2} \leq 0 \end{cases} \tag{34}$$

Equation (34), together with $T_d(0) = 0$ and $T_d(T_r) = T_d^r$ implies

$$T_d(T) = \left(T - \frac{\chi^2}{D}\right) \geq \left(\frac{T_d^r}{T_r}\right) T \tag{35}$$

Simple algebraic manipulations then lead to

$$T\left[\frac{T_r - T_d^r}{T_r}\right] = \frac{T}{T_r}\frac{\chi_r^2}{D} \geq \frac{\chi^2}{D} \tag{36}$$

Therefore, all allowable (χ, T) −paths fulfilling conditions (33) also satisfy:

$$\frac{T}{T_r} \geq \frac{\chi^2}{\chi_r^2} \tag{37}$$

The corresponding time delay is thus given by:

$$T_d = T_d^r \left(\frac{\chi}{\chi_r}\right)^2 \tag{38}$$

Note, that with this particular law the associated damage stress, $(\tau) = \sigma_Y \frac{d\tau_d}{d\tau} = \sigma_Y \frac{T_d\,r}{T_r}$, is constant.

Equations (29) and (38) lead to a new upper bound of the failure energy

$$\Gamma = \gamma(T_r) = \frac{2}{3}\sigma_y \left\{\chi_r T_r - \frac{\chi_r^3}{D}\right\}$$

Thus, the failure energy satisfies:

$$0 < \Gamma < \frac{2}{3}\sigma_y \left\{\chi_r T_r - \frac{\chi_r^3}{D}\right\} \tag{39}$$

For a specified value of Γ, previous expression gives a lower bound for the failure time (Figure 6):

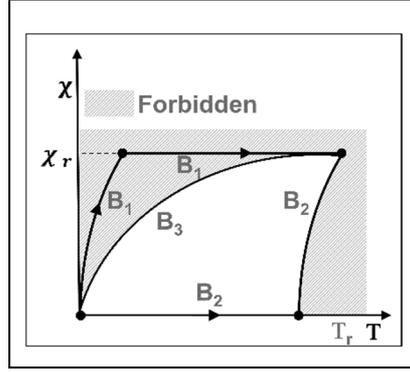$$B_3^r : T_r \geq \frac{\chi_r^2}{D} + \frac{D_2}{2\chi_r} \tag{40}$$

Figure 6: Allowed domain in the (χ, T)-space

The smallest possible failure time allowed by the present physics minimizes expression (40). We call it T_r^{opt} and designate by χ_r^{opt} the corresponding wave front position.

$$\left(\chi_r^{opt}\right)^3 = \frac{DD_2}{4} \quad T_r^{opt} = \frac{3}{4^{(2/3)}}\left(\frac{D_2^2}{D}\right)^{(1/3)} \cong 1.2 \left(\frac{D_2^2}{D}\right)^{(1/3)} \tag{41}$$

3.6. Different trial wave front expressions

The exact solution of the wave front equation (27) is available only if the dissipated power γ' can be expressed as a function of the wave front position which is not easy to realize. Hence, we prefer testing particular relations between time and wave front position. Consistent with the supposition of minimum time to failure for given failure energy, bounds (40, 41) will be considered as the optimum to achieve.

3.6.1. Second order relation between the wave front and time

We consider a second order relation between time and wave front position

$$T = a\chi + b\chi^2 \tag{42}$$

a and b designate parameters determined hereafter. Moreover, we assume that, at failure, the wave front is tangent to a delayed Mott wave $\chi^2 = D(T - T_d^r)$. Hence

$$a = 2\chi_r \left(\frac{1}{D} - b\right) \tag{43}$$

The relation between time delay and failure energy may now be written:

$$\Gamma = \sigma_Y \int_0^{\chi_r} \left[\chi(a + 2b\chi) - \frac{2\chi^2}{D}\right] d\chi$$

The two constants, a and b are given by:

$$a = 2\frac{D_2}{\chi_r^2} \quad \text{and} \quad b = \frac{1}{D} - \frac{D_2}{\chi_r^3} \tag{44}$$

The time at failure depends on the two material characteristics D, D_2 and the failure wave front position:

$$T_r = \frac{D_2}{\chi_r} + \frac{\chi_r^2}{D} \tag{45}$$

We assume now that, for a given failure energy (given D_2) the most likely fracture path minimizes the time to failure. The wave front position, χ_r^{min}, satisfying this assumption depends on the total energy at failure and the material density:

$$\left[\frac{dT_r}{d\chi_r}\right]_{(\chi_r^{min})} = 0 \rightarrow \chi_r^{min} = \left(\frac{DD_2}{2}\right)^{\left(\frac{1}{3}\right)} = 2^{\left(\frac{1}{3}\right)}\chi_r^{opt}$$

Hence, the minimum time to failure predicted by the second order model is:

$$T_r^{min} = \frac{3D_2}{\chi_r^{min}} = 2^{\left(\frac{2}{3}\right)}T_r^{opt} \approx 1.9\left(\frac{D_2^2}{D}\right)^{\left(\frac{1}{3}\right)} \tag{46}$$

The corresponding values of a and b are:

$$a^{min} = 2\left[\frac{4D_2}{D^2}\right]^{(1/3)} \quad \text{and} \quad b^{min} = \frac{-1}{D} \tag{47}$$

Obviously, solution (44) is not close to the bound (40). Thus, we tried a 4th order relation between time and wave front position.

3.6.2. Fourth order relation between the wave front and time

We postulate the following relation between time and wave front position

$$T(X) = a\chi^2 + b\chi^4 \quad for \ \chi \leq \chi_r \tag{48}$$

Assuming moreover that $T(X)$ is tangent to a delayed Mott's wave at failure, implies:

$$b = \frac{1}{2\chi_r^2}\left(\frac{1}{D} - a\right) \tag{49}$$

The energy dissipated to failure the material (29) allows to determine parameter a:

$$\Gamma = \gamma(T_r) = \sigma_Y \int_0^{\chi_r} \chi \frac{dT_d}{d\chi} d\chi = \sigma_Y \left[\frac{4}{15}\chi_r^3\left(a - \frac{1}{D}\right)\right] \tag{50}$$

The two constants, a and b may be written as function of the failure energy, the wave front position at failure (χ_r) and parameters D, D_2:

$$a = \frac{1}{D} + \frac{5D_2}{4\chi_r^3} \quad and \ b = \frac{-5D_2}{8\chi_r^5} \tag{51}$$

Ergo, wave front position and time to failure are related by the following expression:

$$T_r = \frac{\chi_r^2}{D} + \frac{5D_2}{8\chi_r} \tag{52}$$

This solution comes very close to the lower bound (40). The wave front position minimizing the time to failure is:

$$X_r^{min} = \left(\frac{5DD_2}{16}\right)^{(1/3)} = \left(\frac{5}{4}\right)^{\left(\frac{1}{3}\right)}\chi_r^{opt} \tag{53}$$

The minimum time to failure resulting from the 4th order model is:

$$T_r^{min} = \left(\frac{5}{4}\right)^{\left(\frac{2}{3}\right)} T_r^{opt} \tag{55}$$

The results predicted by 4th order relation between T and χ are close to the bounds (40) and (41).

3.6.3. Comparing the different wave paths

Boundary B₃ predicts the minimum time to failure as a function of the wave position. T_r^{opt} and χ_r^{opt} designate respectively the absolute minimum time to failure and the corresponding wave front abscissa.

$$\chi_r^{opt} = \left(\frac{DD_2}{4}\right)^{(1/3)} \quad \text{and } T_r^{opt} = \frac{3}{4^{(2/3)}} \left(\frac{D_2^2}{D}\right)^{(1/3)}$$

The constants D and D_2 follow from invariability of the energy balance with respect to the remote strain rate.

$$D = \frac{2\sigma_y}{\rho} \quad \text{and} \quad D_2 = \frac{3\Gamma}{\sigma_y}$$

Therefore, all the stress release wave models for perfectly plastic materials should predict failure times in the form:

$$\begin{cases} \chi_r \approx \alpha \, \chi_r^{opt} \\ T_r \approx \beta T_r^{opt} \end{cases} \tag{56}$$

α and β are numerical parameters depending on the particular model. Hereafter, to compare the wave paths predicted by the different models, we introduce the non-dimensional variables χ^a and T^a:

$$\begin{cases} \chi^a = \frac{\chi}{\chi_r^{opt}} \\ T^a = \frac{T}{T_r^{opt}} \end{cases} \quad \begin{cases} \chi_r^a = \frac{\chi_r}{\chi_r^{opt}} \\ T_r^a = \frac{T_r}{T_r^{opt}} \end{cases} \tag{57}$$

Table 1 gives the wave coordinates at failure for fixed material parameters. The first column corresponds to the particular model. The second column gives the relation between the time to failure and the wave front position at failure. All the coordinates were normalized by the values corresponding to the absolute minimum time at failure corresponding to the minimum of boundary B₃. The last two columns show the minimum time at failure for each particular model. Evidently, the absolute minimum corresponds to (1,1) on boundary B₃. Figure 7, depicts the same results graphically. The 4th order model gives results very close to the lower boundary B₃.

Model	$T_r^a(\chi_r^a)$	Minimum T_r^a	
		T_r^a	χ_r^a

13

B$_3$	$T_r^a = \dfrac{1}{3}\left[(\chi_r^a)^2 + \dfrac{2}{\chi_r^a}\right]$	1	1
2nd order	$T_r^a = \dfrac{1}{3}\left[(\chi_r^a)^2 + \dfrac{4}{\chi_r^a}\right]$	$(2)^{\left(\frac{2}{3}\right)} \approx 1.6$	$(2)^{\left(\frac{1}{3}\right)} \approx 1.3$
4th order	$T_r^a = \dfrac{1}{3}\left[(\chi_r^a)^2 + \dfrac{5}{2\chi_r^a}\right]$	$\left(\dfrac{5}{4}\right)^{\left(\frac{2}{3}\right)} \approx 1.16$	$\left(\dfrac{5}{4}\right)^{\left(\frac{1}{3}\right)} \approx 1.08$
Grady	$T_r^a = \dfrac{1}{3}\dfrac{(2 + (\chi_r^a)^3)(\chi_r^a)^2}{(\chi_r^a)^3 - 1}$	$(2)^{\left(\frac{2}{3}\right)} \approx 1.6$	$\dfrac{4}{3}(2)^{\left(\frac{1}{3}\right)} \approx 1.68$

Table 1: Normalized time to failure vs normalized wave front abscissa at failure. Minimum time to failure for each model.
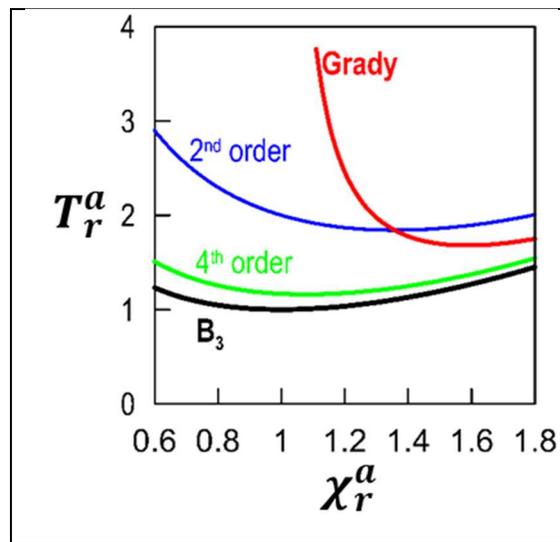

Figure 7: Normalized time to failure vs normalized wave front abscissa at failure for the different models.

Figure 8 illustrates the wave front position for Grady's solution (red), the 2nd order model and the 4th order model. The circles mark final failure. Thus, prior to the circle the different models apply, after the circle a delayed Mott's model is used. Clearly, the new model predicts much smaller wave front positions at failure than Grady's model. Moreover, the time to failure is also much smaller.
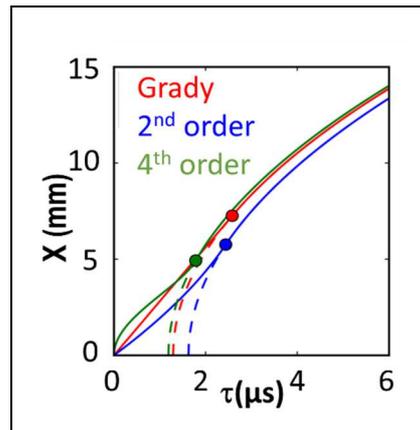
Figure 8: Wave front position in function of time predicted by Grady, 2nd and 4th order model.

4. Conclusion

Broadly, stress release wave propagation controls debris size. Mott was among the first to study the fragmentation process. He considered instantaneous through thickness crack propagation. Hence, the wave front position and time are related by a diffusion equation depending on one physical constant. Based on an ad hoc correction to Mott's approach (progressive drop to zero of the interface stress), some time later, Grady estimated the mean fragment size.

Our present work is based on an energy balance approach. The minimalist assumption of positive energy dissipation related to damage naturally introduces a strong relation between the wave front path and the damage progression.

First, energy conservation for a rod during the process of damage development has been formulated. Then Mott's approach derives naturally as a particular case with no energy dissipation related to damage.

Postulating invariance of the energy balance with respect to the strain rate, defines two characteristic quantities: Mott's diffusion constant D and a new characteristic: length D_2 (depending on the failure energy and yield strength).

Moreover, our energy-based approach also states a residual stress associated to a damage variable. The relation between stress and damage variable is independent of the strain rate. Postulating a decrease of the stress during the damage process gives a new lower bound to the time to failure.

Once the general framework of the damage process was laid out, specific wave front paths were tested. A forth order relation, between the wave front position and time, predicts a failure time and position very close to the lower boundary. The time to failure and the wave front position at failure (characteristic debris size) differ by more than 30 percent from previous models. Therefore; this energy-based approach not only provides the stress damage variable relation, but on a practical side, is far

better at predicting time to failure and in future work will provide a cornerstone to furnish even more accuracy for debris size.

Acknowledgments

References

Cereceda D., Daphalapurkar N., Graham-Brady L., 2017, Modeling dynamic fragmentation of heterogeneous brittle structural materials. Int. J. Impact Eng. 99, 85–101.

Freund L.B., Hutchinson J.W., 1985. High strain-rate crack growth in rate-dependent plastic solids. J. Mech. Phys. Solids Vol. 33, No. 2, pp. 169-191. 1985.

Gao X., Wang T., Kim J., 2005. On ductile fracture initiation toughness: Effects of void volume fraction, void shape and void distribution. International Journal of Solids and Structures 42. 5097-5117.

Grady D.E., 1982. Local inertial effects in dynamic fragmentation. Journal of Applied Physics. 53, 322 (1982); DOI : 10.1063/1.329934.

Grady D.E., 2006. Fragmentation of Rings and Shells - The Legacy of N.F. Mott, Shock wave and pressure phenomena, Springer.

Levy S., 2010. Exploring the physics behind dynamic fragmentation through Parallel Simulations, thesis number 4898, EPFL Lausane.

Levy S., Molinari J. F., I. Vicari I. and Davison A. C., 2010, Dynamic fragmentation of a ring: Predictable fragment mass distributions, Physical Review E82.6: 066105.

Lienau C.C., 1936. Random Fracture of Brittle Solid. J. Franklin Inst., 221, 485-494, 674-686, 769-787.

Mott N.F. and Linfoot E.H., 1943. A theory of Fragmentation. Ministry of Supply, AC3348, January.

Mott N.F., 1943. Fragmentation of Shell Casings and the Theory of Rupture in Metals. Ministry of Supply, AC4613, August.

Mott N.F., 1944. A theory of fragmentation: Application to wire wound bombs 20 lb. Ministry of Supply, AC6338, May.

Mott N.F., 1947. Fragmentation of shell cases, Proc. R. Soc. Lond. A189, 300-308, January.

Nemat-Nasser S., Abé H., Hirakawa S., 1983. Hydraulic fracturing and geothermal energy: Proceedings of the First Japan-United States Joint Seminar on Hydraulic Fracturing and Geothermal Energy, Tokyo, Japan, November 2-5, 1982, and Symposium on Fracture Mechanics

Approach to Hydraulic Fracturing and Geothermal Energy, Sendai, Japan November 8-9, 1982

Tvergaard V., Needleman A., Analysis of the cup and cone fracture in a round tensile bar, Acta Materialia 32 (1984), 157-169.

Taylor G.I., 1963. Volume III, Aerodynamics and the mechanics of projectiles and explosions 44, The fragmentation of tubular bombs, p. 387-390, 1963.

Vocialta M., Molinari J.-F., 2015, Influence of internal impacts between fragments in dynamic brittle tensile fragmentation." International Journal of Solids and Structures 58: 247-256

Zhang H., Ravi-Chandar K., 2006. On the dynamics of necking and fragmentation - I. Real-time and post-mortem observations in Al 6061-O. Int. J. Fract. DOI 10.1007/s10704-006- 9024-7.

Zhang H., Ravi-Chandar K., 2008. On the dynamics of necking and fragmentation - II. Effect of material properties, geometrical constraints and absolute size. Int. J. Fract. DOI 10.1007/s10704-008-9233-3.

Zhou F., Molinari J.-F., Ramesh K., 2005. A cohesive model based fragmentation analysis: effects of strain rate and initial defects distribution. Int. J. Solids Struct. 42 (18), 5181–5207.